*Proceedings of the 2012 IEEE 12th International Conference on Bioinformatics & Bioengineering (BIBE), Larnaca, Cyprus, 11-13 November 2012*

# Measurement of Motion of Carotid Bifurcation Plaques

Hamed Nasrabadi, Marios S. Pattichis
Dept. of Electrical and Computer Engineering
The University of New Mexico
Albuquerque, NM, USA.
{nasrabadi, pattichis}@ece.unm.edu

Perry Fisher
Sophie Davis School of Biomedical Education
Mack Lipkin Fellow 2012
Astoria, NY, USA.
pfisher01@ccny.cuny.edu

Andrew N. Nicolaides, Maura Griffin, Gregory C. Makris
Vascular Screening and Diagnostic Centre
London, U.K.
anicolaides1@gmail.com, maurabgriffin@gmail.com, g.makris09@imperial.ac.uk

Efthyvoulos Kyriacou
Dep. of Computer Science and Eng.
Frederick University
Limassol, Cyprus.
e.kyriacou@frederick.ac.cy

Constantinos S. Pattichis
Dept. of Computer Science
University of Cyprus
Nicosia, Cyprus
pattichi@ucy.ac.cy

***Abstract*—Video loops of B-mode ultrasound images of 35 carotid bifurcation plaques were obtained (4 symptomatic and 31 asymptomatic) from patients with carotid bifurcation atherosclerosis. Video loops were classified visually as showing concordant (n=22) or discordant motion (n=13). Concordant plaques were characterized by uniform orientation of motion throughout the cardiac cycle. Discordant plaques exhibited significant spread in motion orientation at different parts of the cardiac cycle, especially at systole.**

**We developed a real-time motion analysis system that applies Farneback's method to estimate velocities between consecutive video frames. For our purposes, we allow a 100msec time interval between the video frames used in the analysis. This approach allows us to analyze significant motions associated with a larger time interval. Over each video frame, we measure the spread of the motion orientation around the dominant orientation. For each video, we look at the spreads of the motion orientations for different motion magnitudes. Using these motion-spread measurements, we can quantify discordant movement.**

**The sum of maximum fan widths for the median pixel motions 5 to 3 (SMFW5to3) had a median value of 100 degrees and inter-quartile range (IQR) of (80, 110) degrees for the concordant plaques and 270, (230, 430) for the discordant plaques ($P < 0.001$). Thus, we have a new tool to differentiate between concordant and discordant plaques.**

***Index Terms*—Atherosclerosis, Carotid Bifurcation, Ultrasound, Plaque Motion Analysis.**

## I. Introduction

Cardio vascular disease (CVD) is the leading cause of death in the United States. In 2008, CVD was the primary cause of 1 of every 3 deaths or 811,940 of all 2,471,984 deaths in the United States [1]. The prevalence of CVD among American adults is 82,600,000 or greater than 1 in 3. The total direct medical costs of CVD will be tripled from $273 billion to $818 billion between 2010 and 2030. The rate of death by CVD has declined to 30.6% from 1998 to 2008. About 47% of the decrease in death is attributed to increased use of evidence-based medical therapies and 44% to life style and environmental changes. There was a 22% increase in the total number of inpatient cardiovascular operations and procedures, from 6,133,000 to 7,453,000 between 1999 and 2009. In 2008, there were 795,000 cases of new or recurrent stroke and accounted for 1 of every 18 deaths in United States. Among the survivors of ischemic stroke who were older than 65 years, many experience long-term disabilities [1].

The majority of ischemic cardiovascular events are due to atherosclerotic plaques (APs). Thus, B-mode ultrasound of the carotid artery and computed tomography of the coronary artery are used for detecting the presence of atherosclerotic plaques [1]. For symptomatic patients who present transient monocular blindness, transient ischemic attacks or stroke and have a greater than 70% stenosis, carotid endarterectomy (CEA) is the method of choice because it reduces the 5 year stroke rate from 11% to 5% (ECST [2], NASCET [3]). For asymptomatic cases, the decision to remove the plaque depends on the identification of high risk plaques. This is because in patients greater than 70% stenosis CEA reduces the 5 year stroke rate from 2% to 1% as reported in the Asymptomatic Carotid Atherosclerosis Study (ACAS) [4] and ACST [5]. A number of texture features such as a low gray scale median indicating a hypoechoic plaque or the presence of a large juxtaluminal black area without a visible echogenic cap have been shown to be able to identify a high risk subgroup [6]-[8]. However, at best, only 70% of the strokes occurred in this high risk group during follow-up. The remaining strokes occurred in the low risk group.

It has been suggested that plaques may rupture not only as a result of inherent instability, but also due to excessive mechanical forces during the cardiac cycle. Meairs and Hennericci [9] proposed plaque surface motion analysis to distinguish between high and low risk plaques. The approach was based on reconstructions of plaque motions using temporal 3-D (4-D) ultrasound. The authors [9] found significant differences in the maximal discrepant surface velocity (MDSV) motion between symptomatic and asymptomatic plaques. Murillo *et al.* in [10] used a multi-scale AM-FM approach to estimate 2-D plaque motion to help differentiate between symptomatic and asymptomatic cases. More recently, Golemati *et al.* in [11] reported on the differences between average motion measurements extracted from: (i) normal versus elderly, and (ii) symptomatic versus asymptomatic cases.

In this paper, we introduce a new image analysis methodology for quantifying ***discordant*** plaque motion, which is the phenomenon of different parts of the plaque moving in different directions with different velocities during the cardiac cycle. In contrast, ***concordant*** plaque motion is the phenomenon of all parts of the plaque moving in the same direction and the same velocity during the cardiac cycle. Clearly, discordant motion is associated with higher strain, as opposed to concordant motion that is associated with lower values for strain. Our aim is to classify and quantify the motions that can help clinicians differentiate between plaques that are likely to rupture because of high internal strains from plaques with low strains.

The rest of the paper is organized as follows. We describe the methodology in section II. We provide the results in section III and provide concluding remarks in section IV.

## II. METHODOLOGY

A primary goal of the proposed research is to develop an interactive, real-time system that facilitates plaque ultrasound video experimentation. The entire system was implemented using OpenCV libraries [12]. We provide a system diagram with the major components of the system in Fig. 1.

First, each ultrasound video is loaded using an interactive GUI (shown in Fig. 2). The user is then asked to provide a manual segmentation of the initial plaque region. Alternatively, the user can load a pre-computed segmentation of the plaque (see Fig. 2). The user is also asked to provide parameters associated with the motion estimation method and the motion-spread scatterplot analysis. In the following subsections, we provide detailed descriptions of each processing block.

### *A. Ultrasound video acquisition and visual classification*

Video loops of B-mode ultrasound images of 35 carotid bifurcation plaques were obtained (4 symptomatic and 31 asymptomatic) from patients with carotid bifurcation atherosclerosis. Institutional Ethics Committee approval has been obtained. The video loops have been anonymised and studied blind; i.e. without knowledge of presence or absence of symptoms. The ultrasound videos were of size 568x448 pixels at a frame rate of 40 frames per second (fps). 13 plaques were visually classified as showing discordant movement and 22 as showing concordant movement.

From each video loop, we extracted a series of 8-10 consecutive cardiac cycles that did not include any motion artifacts such as carotid movement due to swallowing or neck movement. Video loops were classified visually as mechanically *concordant or discordant*. Here, a plaque was classified as *concordant* if it had all of its components simultaneously move in the same direction throughout the cardiac cycle. On the other hand, a plaque was classified as *discordant* if it had components move in different directions, at certain parts of the cardiac cycle, especially in peak systole.

### *B. Video motion estimation and relevant parameter selection*

Motion estimation is based on Farneback's method [13]. Visually, we have confirmed that this method performs slightly better than Horn and Schunck's method as described in [14]. Over each pixel, the approach fits two local polynomials between two reference video frames. Thus, motion is computed between any two video frames, as opposed to traditional Horn and Schunck's approaches that use averages over several frames [14]. In our motion estimation protocol, as opposed to computing motion between consecutive video frames, we compute the overall motion over a user-specified time interval. This is specified as the $Two\ Frames\ Comparison\ Interval$ parameter in the GUI (see Fig. 2). Here, the interval between different sequential frames compared was set to 0.1 seconds (e.g., $Comparison\ Interval = 4$ frames in a cine loop of 40 fps).

In what follows, we provide more details on the approach. Over each point $x = (x_1, x_2)$ of the video frame, we fit a quadratic polynomial. For the first frame, we have

$$f_1(x) = x^T A_1 x + b_1^T x + c_1, \tag{1}$$

where $A_1$ is a 2x2 real-symmetric matrix, $b_1$ is a 2x1 column vector and $c_1$ is a constant. For computing the parameters in (1), we have a weighted least-squares approach with weights set by a Gaussian of size $N = Expansion\ Window\ Size = 5\ or\ 7$ and with standard deviation $\sigma = Expansion\ Window\ Sigma = 1.2\ or\ 1.5$. For the translation model considered here, at the same pixel in frame 2, we have

$$\begin{aligned} f_2(x) = f_1(x-d) &= (x-d)^T A_1 (x-d) + b_1^T (x-d) + c_1 \\ &= x^T A_1 x + (b_1 - 2A_1 d)^T x + d^T A_1 d - b_1^T d + c_1 \\ &= x^T A_2 x + b_2^T x + c_2 \end{aligned} \tag{2}$$

The relations between polynomial coefficients of the 2nd frame and the 1st frame are given by:

$$A_2 = A_1, \tag{3}$$

$$b_2 = b_1 - 2A_1 d, \tag{4}$$

$$c_2 = d^T A_1 d - b_1^T d + c_1. \tag{5}$$

These coefficients are local functions of each point in the image as given by: $A_1(x)$, $b_1(x)$, $c_1(x)$, $A_2(x)$, $b_2(x)$, and $c_2(x)$. Ideally $A_2(x) = A_1(x)$ as in equation (3) but, here a common $A(x)$ is approximated using

$$A(x) = (A_1(x) + A_2(x))/2. \tag{6}$$

An approximate solution for the displacement $d$ is derived from equation (4) without the need to consider (5). After substituting (6) into (4), we have

$$A(x)d(x) = -\tfrac{1}{2}\big(b_2(x) - b_1(x)\big). \tag{7}$$

The constraint of equation (7) can be solved for $d(x)$ point-wise if $A(x)$ is non-singular but the result can be very noisy. Then, assuming slowly-varying displacements, a Gaussian filter of size $Motion\ Smoothing\ Window\ Size = N =$

$15, \sigma = 0.15 \cdot (N-1)$ is applied to reduce the noise in the estimates.

To capture large displacements, constraint (7) is solved using a coarse to fine approach. At a coarse scale, we get initial estimates of the displacements which are propagated and refined at the finer scales. The number of scales is set by $Pyramid\ Levels = 3$, with downsampling by 2 as we go from scale to scale ($Pyramid\ scale = 0.5$). At the finest scale, estimation is performed at every video pixel. In each scale, the search for a better matching polynomial is done in 3 iterations (Fig. 2, see [13]).

### C. Plaque motion visualization

Statistical analysis of the estimated motion vectors is performed over the region of the plaque. A limitation of the current version of the software comes from the fact that we are not tracking the motion of the plaque boundary throughout the cardiac cycle.

To visualize the motion, the user can select the spacing between the estimated motion vectors ($Motion\ Vectors\ Spacing$) and can also magnify the display of the motion vectors ($Motion\ Vectors\ Magnification$). For larger plaques, we often use a spacing of 10 pixels. For smaller plaques, we use a spacing of 5 pixels. Furthermore, each motion vector is magnified by a factor of 5. We demonstrate our motion visualization in Fig. 3. In Figs 3(c) and 3(d) we show the directional motion distribution (circular histogram plots).

### D. Statistical Analysis

The discrimination between *concordant* and *discordant* motions is based on estimating the motion velocity spread over each video frame, over the entire video. To determine the motion spread, we first find the dominant orientation at each video frame. Here, the dominant orientation is estimated using the peak of the orientation histogram (see Fig. 3(c) and 3(d)). At the dominant orientation, the median velocity magnitude is taken as the $median\_value$ ($y$-axis value) for the scatter-plots (see Fig. 3(e), (f)). For the motion spread, we use the orientation-histogram to determine the angular spread that reaches 50% of the peak orientation (half-peak spread). For each video frame, we have an estimate of the angular spread ($width$) and the $median\_value$ summarized as a single point: $(width, median\_value)$. A collection of all of the points over the entire video is used to generate a scatterplot (see Fig. 3(e) and 3(f)).

We next determine the maximum fan-width for each median value. This is defined using:

$$MAXFW(mval) = \max_{median\_value=mval} width. \quad (8)$$

The maximum fan-width measures the maximum angular spread (in degrees) for a fixed motion magnitude. Here, we bin the motion magnitudes for integer-valued motions $mval$ = 2, 3, 4, and 5 pixels. The sum of the maxima over several integer motions are defined using

$$SMAXFW(mval = i, \dots, j) = \sum_{mval=i}^{mval=j} MAXFW(mval). \quad (9)$$

To differentiate between concordant and non-concordant motions, we examine the sum of the motion spreads as expressed by (9). Here, the basic idea is that non-concordant motions will be characterized by larger spreads.

## III. Results

To differentiate between *concordant* and *disconcordant* motions, we collected ultrasound videos from 35 patients as described in section II.A. These videos were visually classified into concordant plaques ($n$=22) and discordant ($n$=13) plaques.

Figure 3 provides a comparative example between a stable and an unstable case. The orientation histogram of the visually classified as concordant plaque of Fig. 3(c) shows a narrow fan (or wedge) width of 6 degrees at the peak systole of the cardiac cycle. Fig. 3(d) shows the orientation histogram for the visually classified as discordant plaque of Fig. 3(b). In this case, the orientation spread is 84 degrees at the peak systole of the cardiac cycle. The orientation histogram also exhibits 2 distinct peaks suggesting a bi-modal distribution.

We compared the scatterplots for all cases. In Fig. 4, we show the MAXFW and SMAXFW for the different cases described in (8) and (9). From the boxplots, we can see that SMAXFW(i=3,4,5) provides the best separation between stable and unstable plaques. The sum of maximum fan widths for the median pixel motions 5 to 3 (SMFW5to3) had a median value of 100 degrees and inter-quartile range (IQR) of (80, 110) degrees for the concordant plaques and 270, (230, 430) for the discordant plaques ($P < 0.001$). Thus, we have a new tool to differentiate between concordant and discordant plaques.

## IV. Conclusion

Video loops of B-mode ultrasound images of 35 carotid bifurcation plaques were obtained (4 symptomatic and 31 asymptomatic) from patients with carotid bifurcation atherosclerosis. Video loops were classified visually as showing concordant (n=22) or discordant motion (n=13). Concordant plaques were characterized by uniform orientation of motion throughout the cardiac cycle. Discordant plaques exhibited significant spread in motion orientation at different parts of the cardiac cycle, especially at systole.

We developed a real-time motion analysis system that applies Farneback's method to estimate velocities between consecutive video frames. For our purposes, we allow a 100msec time interval between the video frames used in the analysis. This approach allows us to analyze significant motions associated with a larger time interval. Over each video frame, we measure the spread of the motion orientation around the dominant orientation. For each video, we look at the spreads of the motion orientations for different motion magnitudes. Using these motion-spread measurements, we can quantify discordant movement. We are currently testing our approach on larger datasets.

## References


[1] V.L. Roger, A.S. Go, D.M. Lloyd-Jones, E.J. Benjamin, J.D. Berry, *et al.* "Heart disease and stroke statistics—2012 update: a report from the American heart association," *Circulation,* Vol. 125(1), pp. e2-e220, 2012.

[2] The European Carotid Surgery Trialists Collaborative Group, "Risk of stroke in the distribution of an asymptomatic carotid artery," *Lancet,* Vol. 345, pp. 209-212, 1995.

[3] D. Inzitari, M. Eliasziw, P. Gates, B.L. Sharpe, R.K. Chan, *et al.,* "The causes and risk of stroke in patients with asymptomatic internal carotid artery stenosis, North America symptomatic

carotid endarterectomy trial collaborators," *N. Engl. J. Med.,* Vol. 343, pp. 1693-1700, 2000.

[4] Executive Committee for the Asymptomatic Carotid Atherosclerosis Study, "Endarterectomy for asymptomatic carotid artery stenosis," *JAMA*, Vol. 273, No. 18, pp. 1421-1428, 1995.

[5] A. Halliday, A. Mansfield, J. Marro, C. Peto, R. Peto, J. Potter, "Prevention of disabling and fatal strokes by successful carotid endarterectomy in patients without recent neurological symptoms: randomised controlled trial," *Lancet,* Vol. 363, pp. 1491–1502, 2004.

[6] A.N. Nicolaides, S.K. Kakkos, E. Kyriacou, M. Griffin, M. Sabetai, et al., "Asymptomatic internal carotid artery stenosis and cerebrovascular risk stratification," *J. Vasc. Surg.,* Vol. 52, Iss. 6, pp. 1486-1496, 2010.

[7] M.B. Griffin, E. Kyriacou, C. Pattichis, D. Bond, S.K. Kakkos, M. Sabetai, G. Geroulakos, N. Georgiou, C. J. Doré, A. Nicolaides, "Juxtaluminal hypoechoic area in ultrasonic images of carotid plaques and hemispheric symptoms," *J. Vasc. Surg.*, Vol. 52, Iss. 1, pp. 69-76, 2010.

[8] K. Kakkos, M. B. Griffin, A. N. Nicolaides, E. C. Kyriacou, M. M. Sabetai, T. J. Tegos, G. Geroulakos, "The size of juxtaluminal black area in ultrasonic images of asymptomatic carotid plaques predicts the occurrence of stroke," *J. Vasc. Surg.,* Vol.55, Iss. 6, Supplement, pp. 84S-85S, 2012.

[9] S. Meairs, and M. Hennerici, "Four-dimensional ultrasonographic characterization of plaque surface motion in patients with symptomatic and asymptomatic carotid artery stenosis," *Stroke,* Vol. 30, pp. 1807–1813, 1999.

[10] S. Murillo; V. Murray, C. P. Loizou, C. S. Pattichis, M. Pattichis; and E. S. Barriga, "Multi-scale AM-FM motion analysis of ultrasound videos of carotid artery plaques," *Proc. SPIE Medical Imaging. 0001;():832011-832011-10*.

[11] S. Golemati, J. Stoitsis; A. Gastounioti; A. C. Dimopoulos; V. Koropouli; and K. S. Nikita, "Comparison of block matching and differential methods for motion analysis of the carotid artery wall from ultrasound images," *IEEE Trans. Inf. Technol. Biomed.* Vol. 16, No. 5, pp. 852-858, 2012.

[12] OpenCV library, http://opencv.org/.

[13] G. Farnebäck, "Polynomial expansion for orientation and motion estimation," PhD thesis, Linköping University, Sweden, 2002.

[14] B.K.P. Horn and B.G. Schunck, "Determining optical flow," *Artif Intell*, Vol. 17, pp 185-203, 1981.

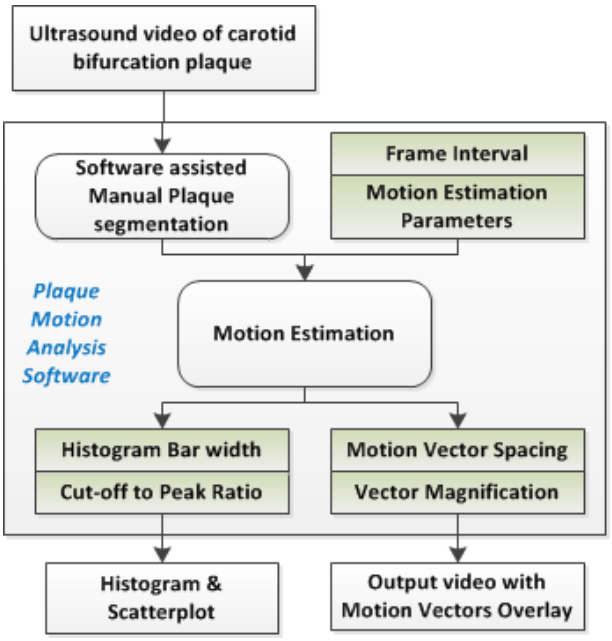


Figure 1. System diagram demonstrating plaque motion analysis software.

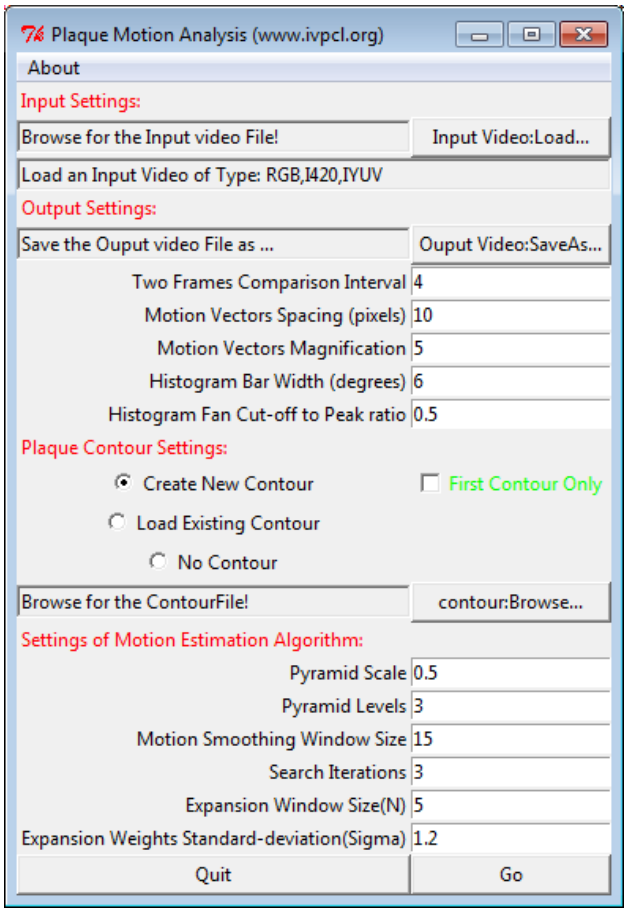


Figure 2. GUI interface for plaque motion analysis.

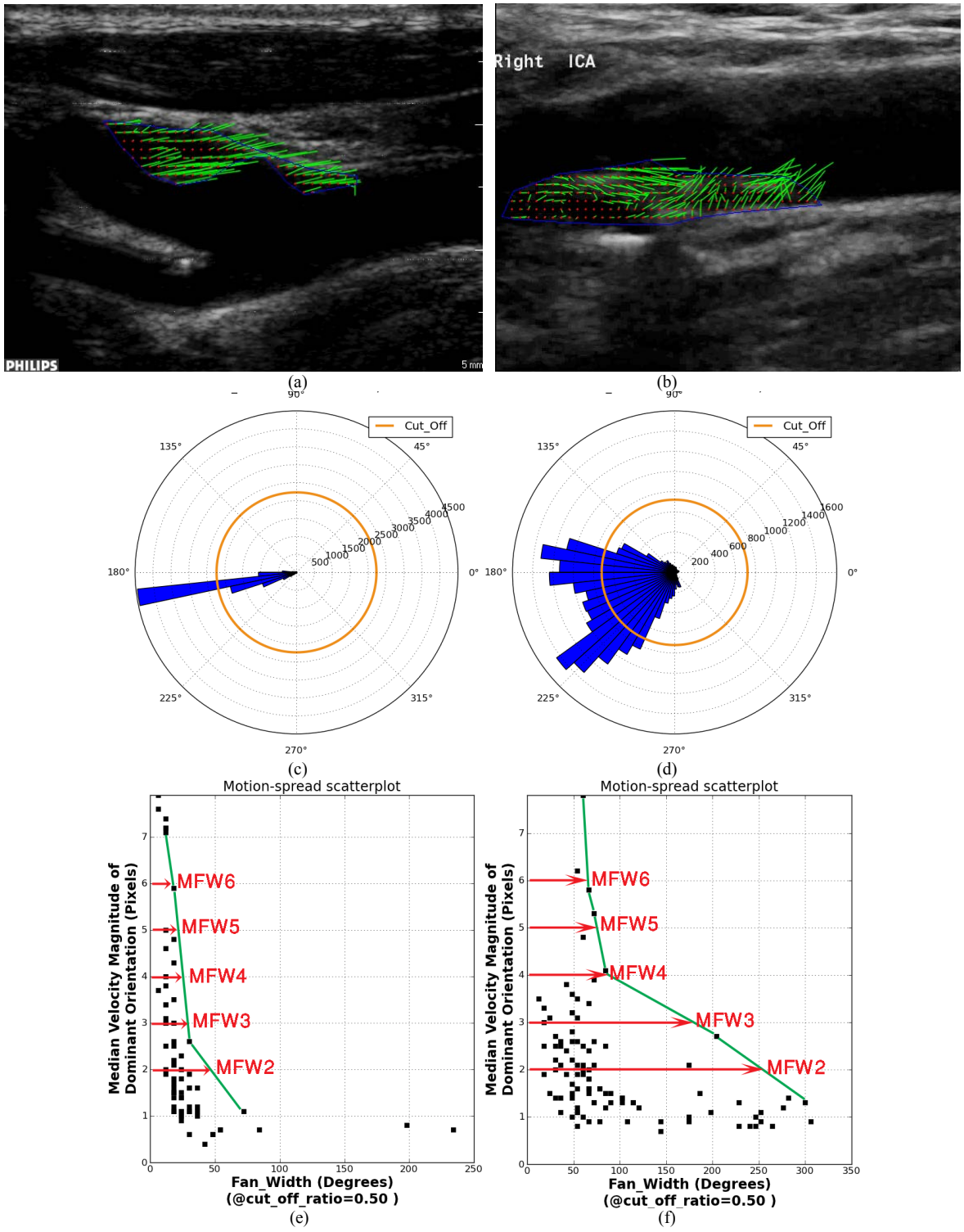


Figure 3. Carotid bifurcation plaque motion analysis. **(a)** Plaque with concordant motion at peak systole. **(b)** Plaque with discordant motion at peak systole. **(c)** Directional motion analysis for concordant plaque demonstrated in (a) for a frame interval of 0.1 seconds. The histogram plot shows the magnitude and orientation. **(d)** Same as in (c) for the discordant plaque demonstrated in (b). **(e)** Motion-spread scatterplot for concordant plaque of (a). There is an obvious uniform motion characteristic from a maximum displacement of 7 pixels down to 2. **(f)** Motion-spread scatterplot for the discordant plaque of (b). There is a characteristic wide fan-width for peak motion of 6 pixels down to 2.

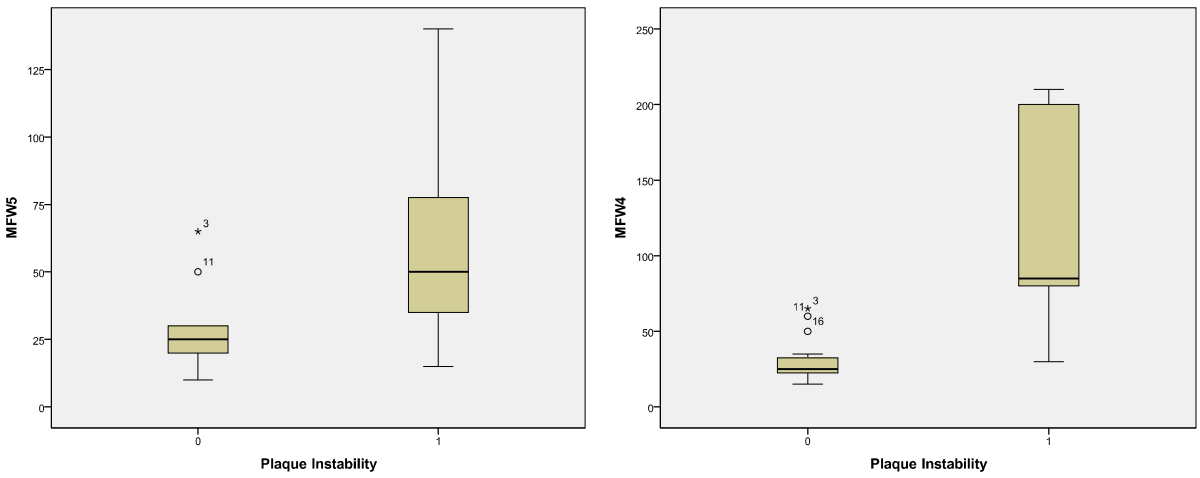


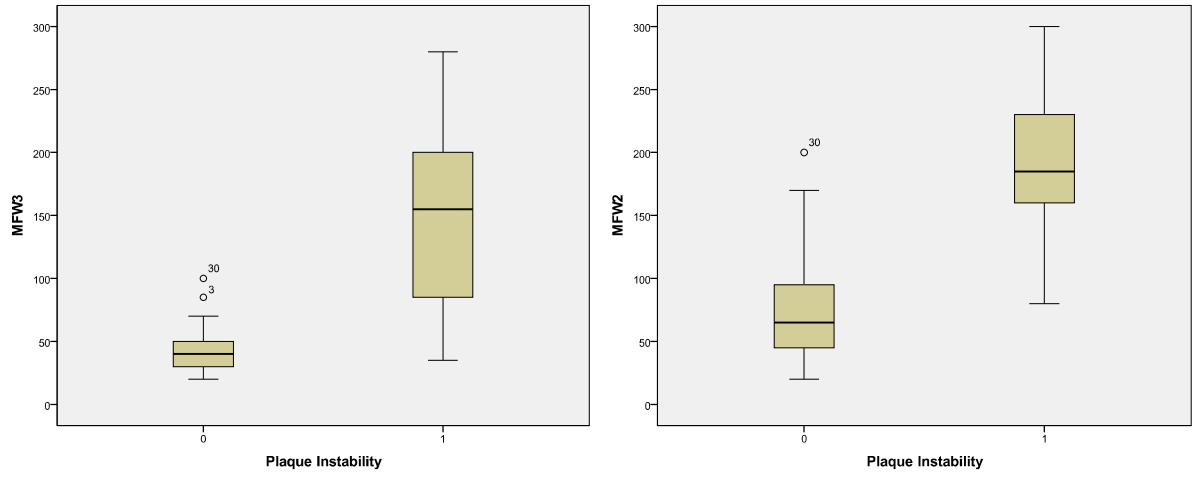


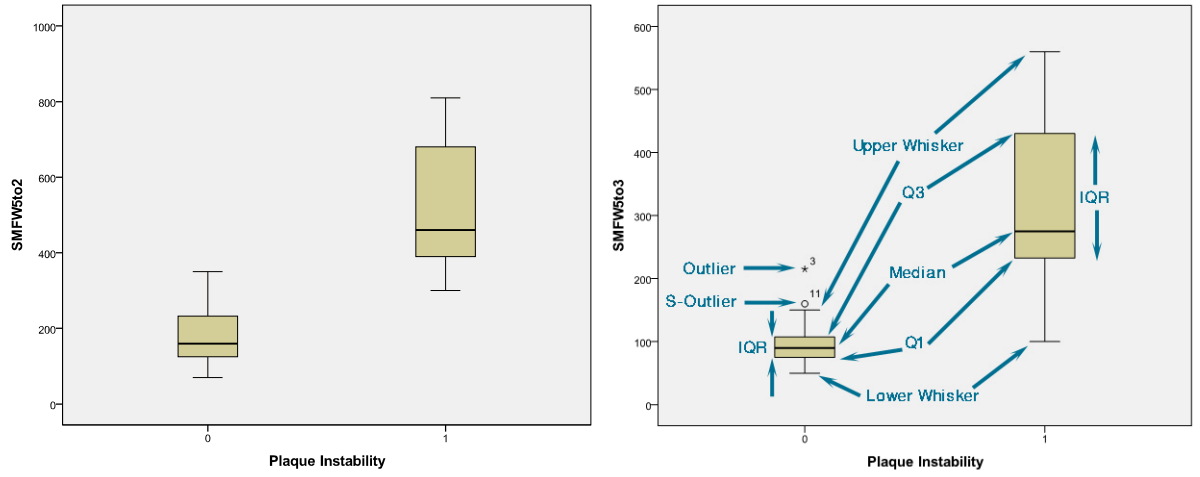


Figure 4. Boxplots of the maximum fan-width (MAXFW in (8)) and the sum of the maximum fan widths (SMAXFW in (9)) for different, integer pixel motions. Here, "0" refers to stable plaques and "1" refers to "unstable" plaques. **(a)** Boxplot for MAXFW(5). **(b)** Boxplot for MAXFW(4). **(c)** Boxplot for MAXFW(3). **(d)** Boxplot for MAXFW(2). **(e)** Boxplot for SMAXFW(i=2,3,4,5). **(f)** Boxplot for SMAXFW(i=3,4,5).
Boxplot Legend. Q1/Q3: 1st/3rd quartile or 25th/75th percentile shown as the lower/upper hinge of the box. M: median shown as a line segment across the box. IQR: interquartile range is the box height from Q1 to Q3. Lower/Upper Whisker: The smallest/largest observed value within 1.5×IQR below/above the Q1/Q3. S-Outlier: Suspected outliers shown by unfilled circles are between 1.5×IQR to 3×IQR below/above Q1/Q3. Outlier: Outliers shown by 5-pointed stars are 3×IQR or more below/above the Q1/Q3. The outliers are labelled by the identifying numbers.